Original Article

Institution of MECHANICAL ENGINEERS
Journal of POWER AND ENERGY

Proc IMechE Part A:
J Power and Energy
0(0) 1–16

DOI: 10.1177/0957650918787077
journals.sagepub.com/home/pia
SAGE

Characteristic of a multistage reheating radial inflow in supercritical compressed air energy storage with variable operating parameters

Hui Li[1], Wen Li[1,2], Xuehui Zhang[1], Yangli Zhu[1], Zhitao Zuo[1], Wei Qin[3] and Haisheng Chen[1,2]

Abstract

In the present study, aerodynamic performance of a four-stage reheating radial inflow turbine, which is adopted in the 1.5 MW supercritical compressed air energy storage system, is analyzed by using the method of integral numerical calculation. Results illustrate that when the inlet total pressure of the first stage is decreased, the expansion ratio of the fourth stage decreases the most. System isentropic efficiency decreases about 1% when the inlet total pressure of the first stage is changed from 7 MPa to 3 MPa, and the fourth stage's isentropic efficiency decreases about 7%. When the rotational speed is decreased, isentropic efficiency and total power decrease gradually and isentropic efficiency changes from 90.5% at 110% speed ratio to 71.1% at 60% speed ratio. Increasing reheating temperature results to the decrease of mass flow rate and isentropic efficiency and the increase of total power. Total power increases by about 105% when the reheating temperature is changed from 60 °C to 520 °C. When the guide vane opening of the first stage is increased, the expansion ratio of the first stage shows different trends compared to other stages and mass flow rates, and total power are proportional to the guide vane opening. System isentropic efficiency decreases by about 4% when the guide vane opening is adjusted from 80% to 30%.

Keywords

Supercritical compressed air energy storage, aerodynamic performance, multistage, variable operating parameters, radial inflow turbine

Date received: 27 December 2017; accepted: 30 May 2018

Introduction

In recent years, energy storage has become a more and more important tool for energy utilization.[1,2] For large-scale energy storage, compressed air energy storage (CAES) and pumped storage are the two main feasible methods.[3–5] Compared to pumped storage, CAES has the advantages of fewer environmental restrictions, fewer construction costs, and so on.[6] Considerable theoretical research and demonstration projects have been conducted, which indicates a bright future for CAES.

As a key part of the CAES, turbo-expander has a significant impact on the system. Axial and radial inflow turbines are the two main common kinds of turbines used in CAES. Compared to an axial turbine, the main advantages of a radial inflow turbine are its higher expansion ratio and higher efficiency at small mass flow rates. Radial inflow turbines have been widely used in aircraft auxiliary power units, cryogenic expanders and automotive turbochargers.[7] To meet the requirements of higher expansion ratios, multistage radial inflow turbines are further used in the waste heat and pressure recovery, solar thermal power, CAES, and so on.[8–10]

The performance of a multistage radial inflow turbine is mainly affected by the aerodynamic performances of each stage and the compatibility of the adjacent two stages. For a single-stage radial inflow

[1]Institute of Engineering Thermophysics, Chinese Academy of Sciences, Beijing, PR China
[2]University of Chinese Academy of Sciences, Beijing, PR China
[3]Institute of Mechanics, Chinese Academy of Sciences, Beijing, PR China

Corresponding author:
Wen Li, Institute of Engineering Thermophysics, University of Chinese Academy of Sciences, Beijing 100190, PR China.
Email: liwen@iet.cn

turbine, the influences of impeller size, vane number, and tip clearance on the efficiency of radial inflow turbines were investigated by Hiett and Johnston.[11] Kofskey and Haas[12] researched the influence of load on the efficiency of radial inflow turbines. Impacts of area change rate of the impeller passage, impeller outlet diameter, and tip clearance on the efficiency of radial inflow turbines were revealed by Watanabe et al.[13] Simonyi et al.[14] designed a compact radial inflow turbine, which was experimentally studied. Jones designed a high expansion ratio radial inflow turbine, and its overall performance was also studied experimentally. Concerning multistage radial inflow turbines, a three-stage radial inflow turbine with a steam working medium was simulated and analyzed by Li and Zheng.[15] He also studied the influence of the admission on the multistage radial inflow turbines.[16] Both numerical and experimental performance maps of an ORC radial inflow two-stage turbine were researched by Hamdi et al.[17] A four-stage radial inflow turbine with inter-stage reheaters of the first 1.5 MW supercritical compressed air energy storage system (SCAES) system was designed and researched by Zhang et al.[18,19] The turbines and inter-stage reheaters are shown in Figure 1. Zhang et al.'s work was mainly concern on the experiment and rated calculation results.

Inter-stage reheaters are used in SCAES system, while they are not employed by the traditional multistage radial inflow turbines. Additionally, large total expansion ratio and the same reheated temperature are the two main special characteristics of the SCAES system. However, the SCAES system often does not operate under its rated conditions and variable operating characteristics of the multistage reheating radial inflow turbine in the system are still unknown. Further study of the variable operating characteristics of this multistage reheating radial inflow turbine should be conducted by computational fluid dynamics (CFD).

Traditional numerical research methods on multistage reheating radial inflow turbines require many calculations for variable operating conditions at each stage. Inter-stage parameter-matching of the adjacent two stages can be achieved according to each stage's characteristic curves. However, too much time is required by this method for a single operation condition. In addition, variations of inter-stage reheaters pressure loss at variable operating conditions cannot be considered with the traditional methods.

To overcome the disadvantages of traditional numerical research methods, an integral numerical calculation method is provided in this paper for investigating the multistage reheating radial inflow turbine. Multistage radial inflow turbines and inter-stage reheaters are included in the numerical simulation. Mass flow rate, expansion ratio, and isentropic efficiency of each stage can be achieved through one numerical calculation cycle. For the multistage reheating radial inflow turbine, mass flow rate, expansion ratio, and isentropic efficiency of each stage will be changed with the inlet total pressure of the first stage, rotational speed, reheating temperature, guide vane opening, and so on. The overall characteristics and internal flow characteristics of these variable operating conditions are investigated in this paper.

Figure 1. Four-stage reheating radial inflow turbine.

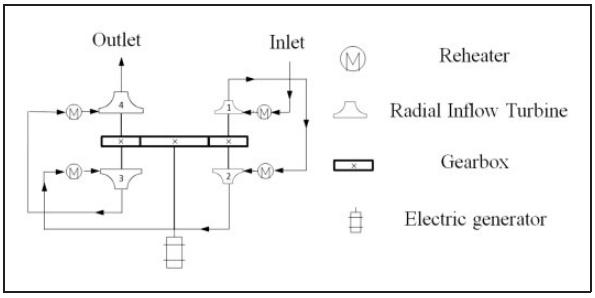

Figure 2. Schematic diagram of the multistage reheating radial inflow turbine.

Research object and methods

Research object

The turbo-expander system, which is used in the 1.5 MW SCAES system, includes four-stage radial inflow turbines and inter-stage reheaters and is shown in Figure 2. Inter-stage reheaters are installed before the expander of each stage. The first- and second-stage turbines are installed at the ends of a shaft by a "back-to-back" method. The same arrangement is used for the third- and fourth-stage turbines. These two shafts and a spindle are contacted by a gear, which is in the middle of the shaft. The generator is driven by the principal axis of the gearbox. Compressed air is first reheated in the reheaters, and then enters the expanders for expansion.

The guide vanes of the first and third stages are adjustable and they are used to adjust the expansion ratio of each stage to obtain a better expansion ratio distribution of each stage. In order to reduce the rotor

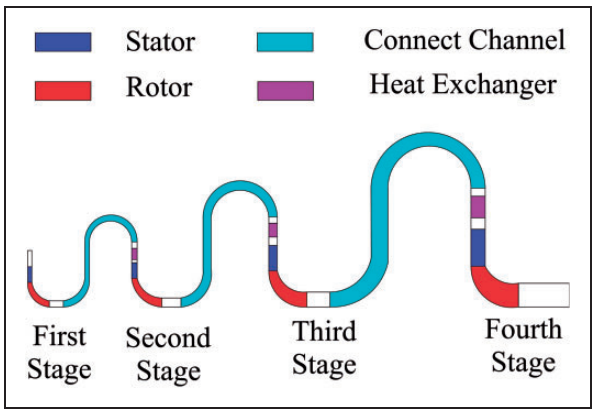

Figure 3. Model diagram of numerical simulation of multi-stage radial inflow turbine.

Table 1. Guide vane and rotor numbers of each stage.

	First stage	Second stage	Third stage	Fourth stage
Guide vane number	10	8	8	8
Rotor number	15	15	22	17

Table 2. Geometric parameters of each stage.

	First stage	Second stage	Third stage	Fourth stage
a (mm)	188.2	214.7	486.7	481.9
b (mm)	143.2	140.8	316.2	312
c (mm)	135	135	305	305
d (mm)	5.0	9.5	10	30
e (mm)	34.0	32	70	86
f (mm)	58.2	45	123	79.4
g (mm)	76.9	91.4	172	220.4

tip clearance leakage flow loss under high pressure, shrouded blades are used for the first and second stages.

CFD calculation method

The numerical model used in this paper is depicted in Figure 3. Four-stage expanders are connected by "connect channels" in a specific sequence. Shaft directions of all of the expanders are specified along the *Z*-axis. Rotational speeds for these four expanders are specified in accordance with the actual operation condition. Inter-stage reheaters are also included in the "connect channels" to provide reheated temperature. Guide vane and rotor numbers of each stage are shown in Table 1. Geometric parameters of each stage are shown in Table 2. Figure 4 shows a schematic of the guide vane and rotor. The four-stage rotors are shown in Figure 5.

Total number of cells is about 4.4 million after the independent verification. Computational cells of

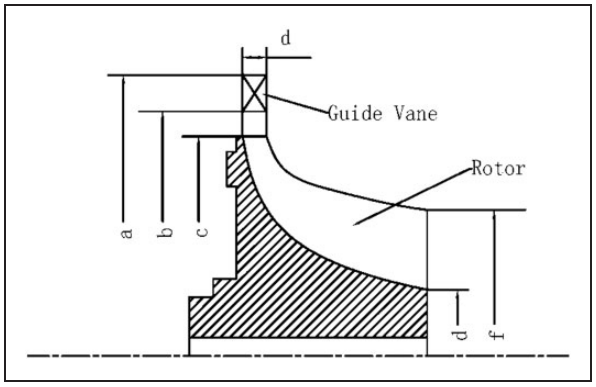

Figure 4. Schematic of the guide vane and rotor.

the multistage reheating radial inflow turbine are shown in Figure 6.

If the plate-fin heat exchanger is simulated directly, cell generation is a tough task. In addition, if cell number is large, a long time is required for the calculation. To solve this problem, a porous media model is used to simulate the plate-fin heat exchanger.[20] This method has been used since the 1970s and calculation results proved it to be effective and accurate.

Performance of the system and each stage are the main focus of this paper, so the inter-stage reheaters are not a key part. Only the inter-stage temperature increases and pressure drops need to be primary considerations for the numerical simulation. In order to simplify the computational geometry, the plate-fin reheaters shape is changed. Even though this change may lead to the increase of computational errors, the revision of loss coefficient in porous media can reduce errors. Moreover, the value of reheater pressure drop is small compared to the internal pressure drop of each stage and its accuracy requirement is not high.

A directional loss mode is used for the nonuniformity of fluid velocity. Loss coefficient is employed to control the inter-stage pressure loss. For the inter-stage temperature increase, total heating value is given to match the requirement.

CFX 12.1 is applied for the numerical simulation. Turbulence model of finite volume, finite volume method, and second-order upwind scheme are used in the mathematical calculation. Multi-grid is used for the calculation accelerating convergence. No-slip and adiabatic boundary are used on the wall. And circumferential averaging flow value method is imposed to transfer data between the guide vane and rotor. A total energy model is used for heat transfer of governing equation. This mode is used to solve the transport of enthalpy and the influence of kinetic energy has been considered. Stage method is used to transfer data between stator and rotor. The y^+ value is required to be between 30 and 300 for the k–ε turbulence model, where the first layer mesh thickness should be adjusted to keep most y^+ within this range. For the calculation material, a real air property table generated by the CFX-TASC flow is employed.

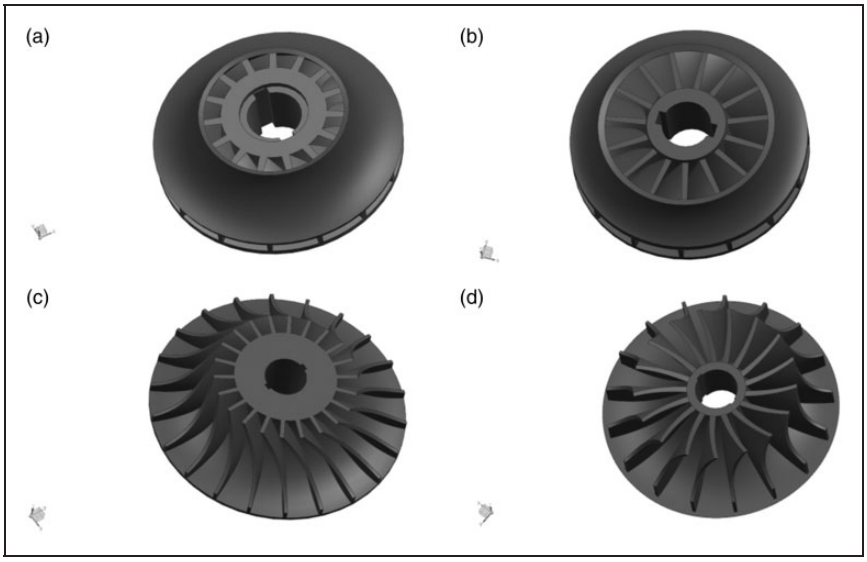

Figure 5. Rotors of four stages: (a) first stage; (b) second stage; (c) third stage; and (d) fourth stage.

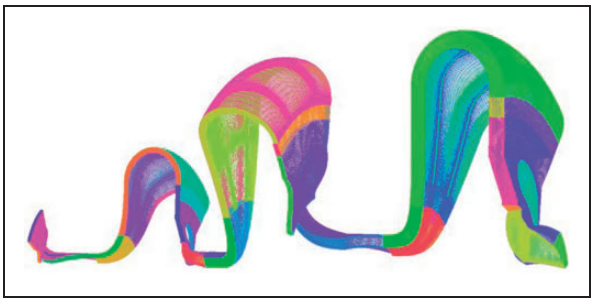

Figure 6. Computational grid of multistage reheating radial inflow turbine.

Table 3. The main boundary condition of calculation.

Inlet total pressure	4–7 MPa
Inlet total temperature	120°C
Outlet static pressure	96 kPa
Rotational speeds of first and second stages	36,000 r/min
Rotational speeds of third and fourth stages	18,000 r/min

At the inlet boundary of first stage, total pressure, total temperature, and circumferential flow angle are given. At the outlet boundary of last (fourth) stage, average static pressure is imposed.

Validation of numerical methodology

In order to verify the validation of the numerical simulation methodology in this paper, the calculation results are compared with the experimental results for the 1.5 MW SCAES. The main boundary conditions are shown in Table 3.

For the experiment, when the turbine system is started, the rotational speed of the first stage increases from 0 to 36,000 r/min and the inlet total pressure changes from 0 to 4 MPa in about 5 min. Meanwhile, inlet total temperature of each stage can be kept in a certain range. Then inlet total pressure changes from 4 to 7 MPa and the rotational speed, and inlet total temperature stay almost constant. Expansion ratio and power can be obtained in the process.

Calculation results and experimental results are shown in Figure 7. From Figure 7(a), it is clear that the same trend is shown for the expansion ratios of four stages. However, the values of the numerical calculation are a little higher than the experimental results except the fourth stage. The differences between the numerical calculation and experiment mainly derive from two reasons. Firstly, some parts with little pressure loss are not included in the calculation. Secondly, the steady state is used in the numerical calculation and the experiment process is a relative steady-state condition. The same trend for power is shown in Figure 7(b). In general, the calculation and experimental results matches well, which means that the numerical simulation is reliable.

Performance and analysis at variable operating conditions

Compared to the rated condition, variable operating conditions are more complex and need to be investigated. Moreover, SCAES system does not always operate under the rated condition for different power and efficiency requirements. To investigate the influences of variable operating conditions on the overall performance and the internal flow characteristics of the multistage reheating radial inflow turbine, four kinds of variable operating conditions are investigated. These conditions include the change of the inlet total pressure of the first stage, rotational speed, reheating temperature, and guide vane opening.

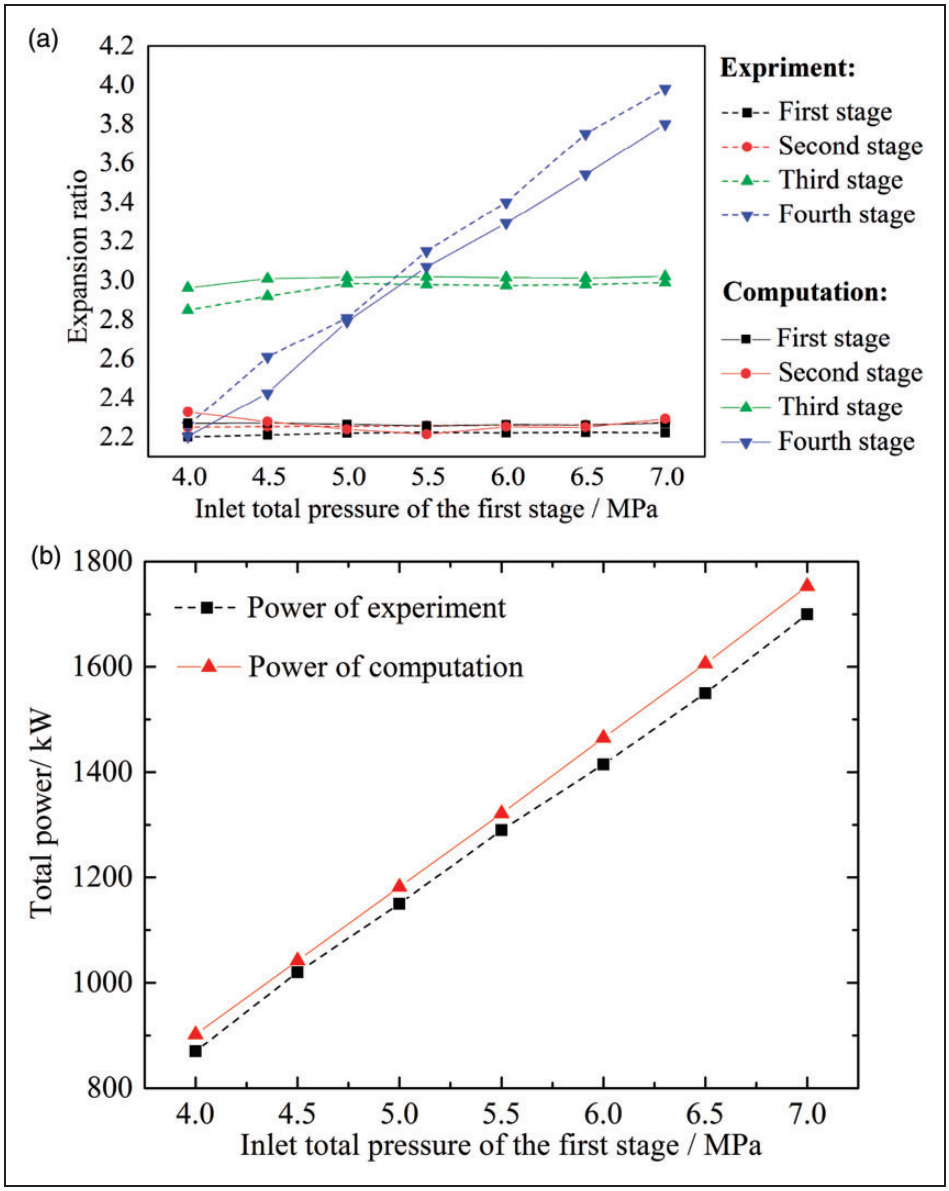

Figure 7. The results of numerical calculation and experiment: (a) expansion ratio of each stage; and (b) total power.

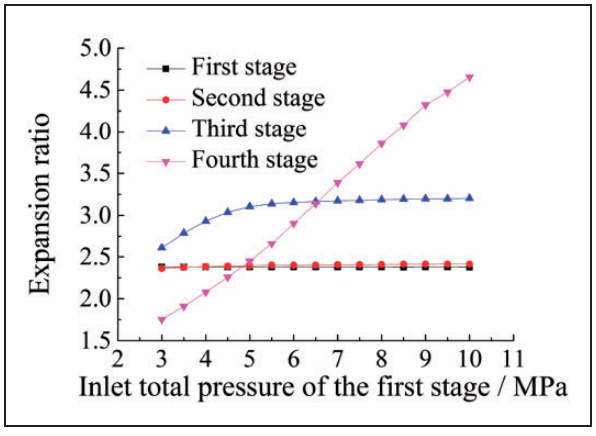

Figure 8. Variation of the expansion ratio with the inlet total pressure of the first stage.

Effect of the inlet total pressure of the first stage

During the running of a SCAES system, pressure of the gasholder will be decreased with the time, which leads to the drop of the inlet total pressure of the first stage. The expansion ratios of each stage will be redistributed and efficiencies as well as powers will be changed at the same time.

Figure 8 shows the expansion ratios of each stage under different inlet total pressures of the first stage. It can be seen that there is little change for the first two stages. However, the third-stage expansion ratio increases with the inlet total pressure of the first stage when it is below 5.5 MPa. Guide vane channel cross section is the same as Laval nozzle. When the

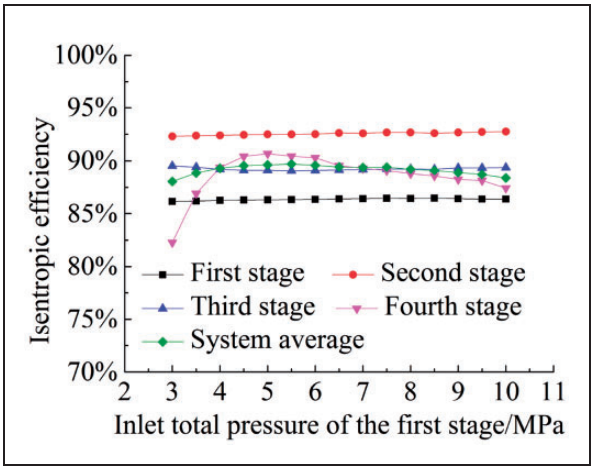

Figure 9. Variation of isentropic efficiency with the inlet total pressure of the first stage.

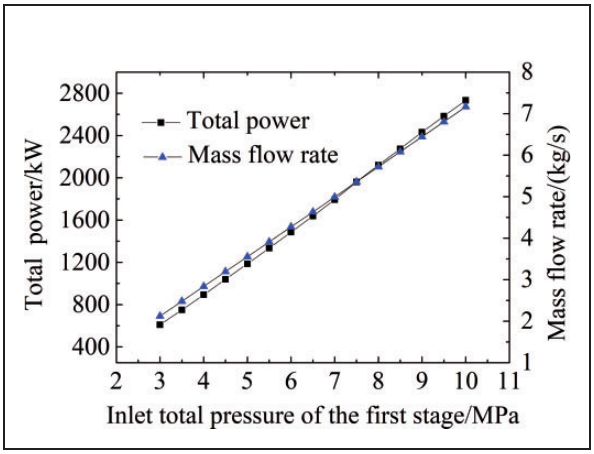

Figure 10. Variation of total power and mass flow rate with the inlet total pressure of the first stage.

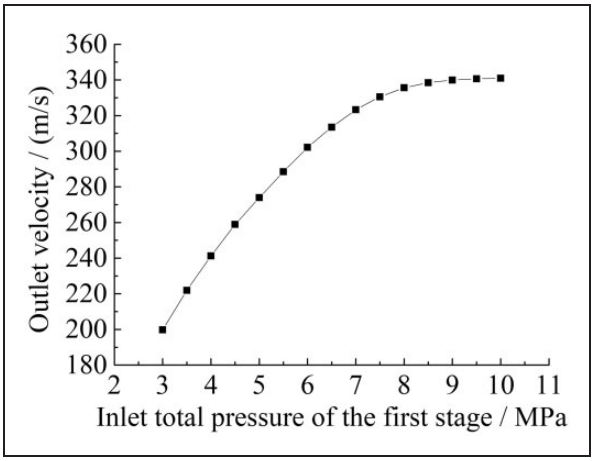

Figure 11. Outlet velocity of the fourth stage with the inlet total pressure of the first stage.

first stage inlet total pressure is above 5.5 MPa, with the increasing of pressure, the flow velocities in four-stage guide vane channels are supersonic, which leads to the inlet total pressures of each stage change linearly and the expansion ratios of the first three stages are almost invariable. When the first-stage inlet total pressure is below 5.5 MPa, with the increasing of pressure, the flow velocity in the fourth-stage channel vane is subsonic. For the third stage, the increase in the inlet total pressure is less than the fourth stage, which leads to the decrease in the expansion ratio of the third stage. As to the fourth stage, the expansion ratio keeps increasing with the inlet total pressure, which is due to the unchanged outlet total pressure of this stage.

The system average isentropic efficiency is defined as

$$\eta_{tot-isp} = \frac{\sum_{n=1}^{4} \Delta H_n}{\sum_{n=1}^{4} \Delta H_{isp-n}} \quad (1)$$

where ΔH_n is the enthalpy drop of each stage and $\Delta H_{isp\text{-}n}$ is the isentropic enthalpy drop of each stage.

Figure 9 reveals the isentropic efficiency changes with different inlet total pressures of the first stage. It is clear that the varieties of the isentropic efficiencies of the first three stages can be neglected. The expansion ratios of these stages are around the optimal values following the increase of the inlet total pressure. In this condition, enthalpy and isentropic enthalpy are mainly related to the expansion ratio and the influence of inlet total pressure can be negligible. Isentropic efficiency of the fourth stage decreases with the inlet total pressure of the first stage when it is less than 4 MPa or above 6 MPa. This decrease is more obvious when the pressure is less than 4 MPa. When the expansion ratio of the fourth stage is beyond the optimal expansion ratio, a significant loss increase can be seen, particularly in small values, which leads to the drop of isentropic efficiency. The loss will be explained in detail later. System average isentropic efficiency has a similar trend with the fourth stage in a smaller changing scale, since the ratio of the fourth-stage power to the total power decreases rapidly when the inlet total pressure of the first stage is below 4 MPa.

Figure 10 represents the mass flow rate and total power with different inlet total pressures of the first stage. It can be seen that the mass flow rate and total power increase linearly with the inlet total pressure of the first stage. For the variety of mass flow rate, it is in direct proportion to the inlet total pressure of the first stage when the flow in the guide vane of the first stage reaches a critical condition with ideal gas. Although this relationship is obtained with ideal gas theory, error using this conclusion with real air is small and the result is acceptable. For the variation of total power, this mainly results from the linear trend of mass flow rate. Strictly speaking, total power and inlet total pressure of the first stage do not display a linear relationship, which results from the system per unit mass power decreasing with the inlet total pressure of the first stage. However, as the decrease is a small value compared to the mass flow rate, an

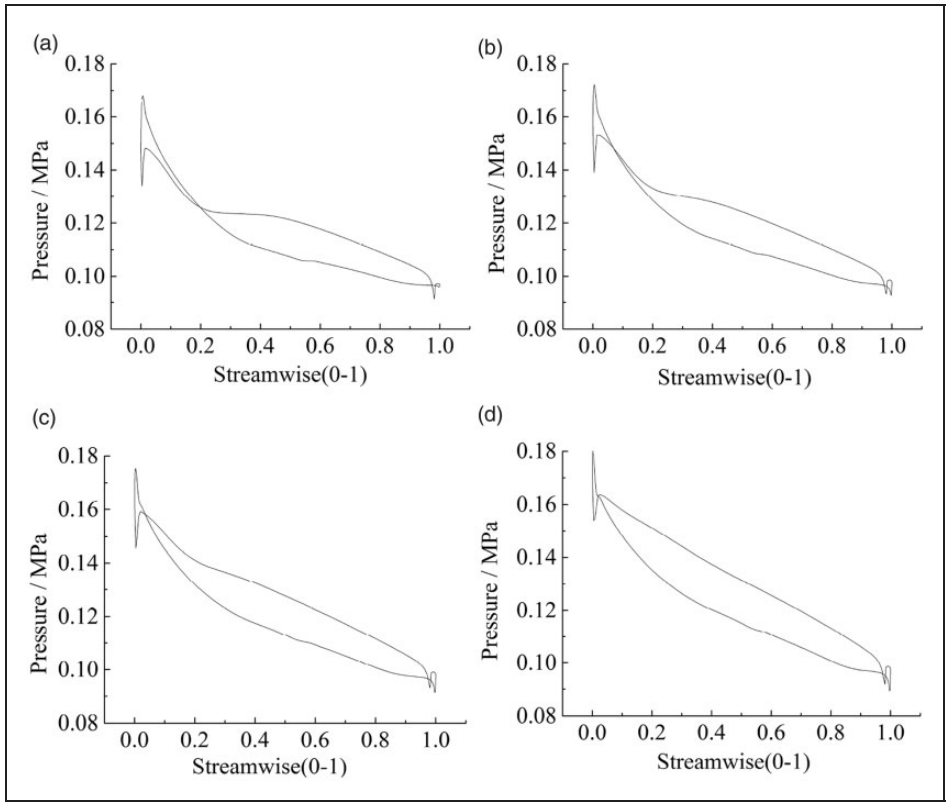

Figure 12. The load of 50% blade height with different inlet total pressures of the first stage: (a) 3 MPa; (b) 3.5 MPa; (c) 4 MPa; and (d) 4.5 MPa.

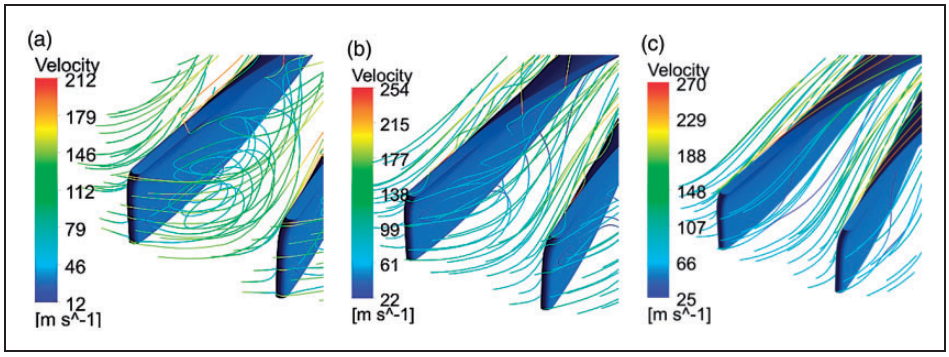

Figure 13. Rotor channel 3D fluid stream: (a) 3 MPa; (b) 4 MPa; and (c) 5 MPa.

approximate linear relationship is shown for the total power and the inlet total pressure of the first stage in Figure 10.

Expansion ratio and isentropic efficiency of the fourth stage change more than the other three stages, so the internal flow characteristics of the fourth stage will be investigated next. First, guide vane channel internal flow is investigated. It can be seen that the outlet angle changes little with the inlet total pressure of the first stage, only increasing from 75.7° at 3 MPa to 76.4° at 10 MPa. However, outlet velocity has a different trend, as shown in Figure 11. Its increasing rate declines gradually with the increasing inlet total pressure. Outlet velocity is about 340 m/s when the inlet total pressure is above 8 MPa.

Efficiency of the fourth stage has an obvious drop when the inlet total pressure of the first stage is below 4 MPa. Static pressure distribution at 50% rotor blade height of the fourth stage is shown in Figure 12. It is clear that the load deterioration occurs at the first 20% area of rotor channel. To analyze this phenomenon, the 3D streamline of rotor channel is investigated, as shown in Figure 13. There is an obvious vortex at the inlet part of rotor channel, which is due to the mismatching between the rotor's linear velocity and the guide vane channel outlet flow's circumferential velocity. When inlet total pressure is lower, the vortex is larger and the load deterioration is more serious.

Pressure on the pressure surface is even lower than that of the suction surface at the inlet part, which

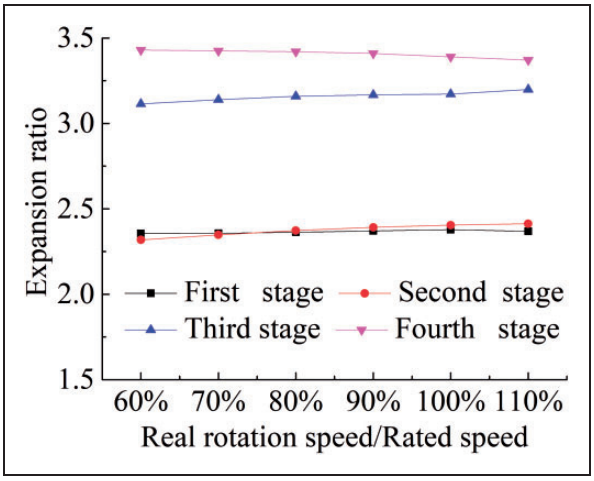

Figure 14. Variation of expansion ratio with rotational speed ratio.

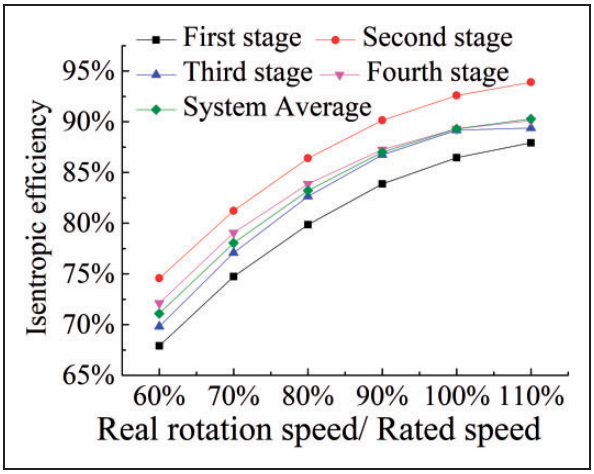

Figure 15. Variation of isentropic efficiency and power with rotational speed.

leads to the blades consuming power. This phenomenon is more obvious and deterioration area is larger when the inlet total pressure is lower. This leads to the obvious drop of efficiency when the inlet total pressure of the first stage is lower than 4 MPa.

When the inlet total pressure is above 6 MPa, the mismatching of the rotor's linear velocity and guide vane channel outlet flow's circumferential velocity is small and the internal flow of rotor channel is uniform. The efficiency drop is mainly due to the increasing friction loss between the channel surface and flow.

Effect of rotational speed

Rotational speed has a significant influence on the power and isentropic efficiency. To investigate this relationship, several conditions of rotational speed ratio from 60% to 110% are calculated and analyzed.

Figure 14 illustrates the relationship between the expansion ratios of each stage and the rotational

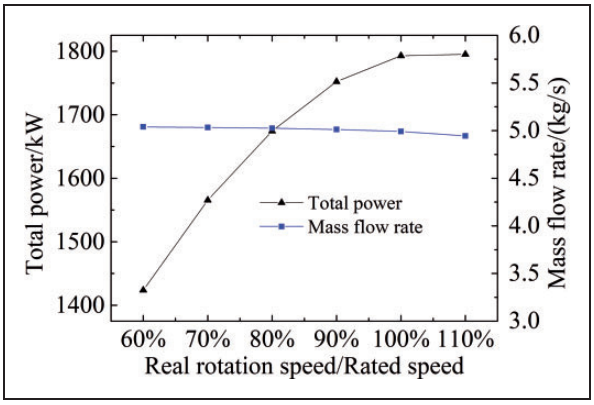

Figure 16. Variation of total power and mass flow rate with the rotational speed.

speeds. It is clear that the changes of expansion ratio of each stage are small during the variation of rotational speed, which results from the system mass flow rate remaining constant almost across different rotational speeds. Flow in the guide vane channel throat reaches a critical condition and mass flow rate is almost in direct proportion to the inlet total pressure, so the inlet total pressures of each stage change little according to the mass conservation law. Expansion ratios of each stage also change little.

Figure 15 illustrates the isentropic efficiencies across different rotational speeds. Efficiencies increase with higher rotational speed. As the rated rotational speed is less than the optimal rotational velocity, incidence loss increases as the rotational speed is reduced. Moreover, as the expansion ratios of each stage change little, isentropic enthalpy drops of each stage also change little. For these two factors, isentropic efficiencies of each stage increase with the increasing rotational speed. Since each stage has the same trend, system average isentropic efficiency also becomes smaller with lower rotational speeds.

Figure 16 represents the mass flow rate and total power with different rotational speeds. From this, it can be seen that mass flow rate is almost invariable when the speed is changed, which results from the fact that that the flow in the guide vane throat of the first stage reaches a critical condition and the inlet total temperature as well as total pressure of first stage do not change. Meanwhile, the total power increases with the increasing rotational speed. As to the little change of isentropic powers and mass flow rate, total power shows a similar trend to the system isentropic efficiency.

When the rotational speed is reduced, variations of the expansion ratios of the four stages are little. In addition, inlet total temperature does not change, so guide vane channel outlet velocity and flow angle are almost constant.

When the rotational speed is reduced, disagreement between guide vane channel outlet fluid's circumferential velocity and rotor's inlet circumferential speed increases gradually. In this condition, fluid velocity

has a sharp rise when it rounds the leading edge and enters the suction surface side, as shown in Figure 17. A vortex is generated near the suction surface at the inlet part of the rotor channel. This vortex moves towards the pressure surface and disappears at the corner between the pressure surface and the shroud. The vortex leads to the deterioration of fluid and the loss increasing, as shown in Figure 18. When the rotational speed is less, loss near the suction surface at the inlet part of the channel is larger. This phenomenon is especially obvious when the rotational speed is below 80% rated speed.

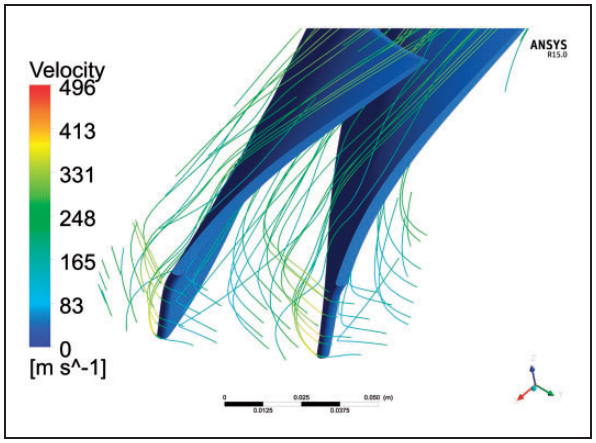

Figure 17. Rotor channel 3D fluid stream at 60% rotational speed.

Effect of reheating temperature

No inter-stage reheaters are applied in the early CAES system. To use the compression heat from the compressor, reheaters are installed before the expander of each stage in SCAES system. In this condition, inlet temperatures of each stage and the available total enthalpy drops will be increased, which leads to more power.

In addition to the compression heat from the compressor of CAES system, there are other heat sources with different conditions, such as the industrial waste

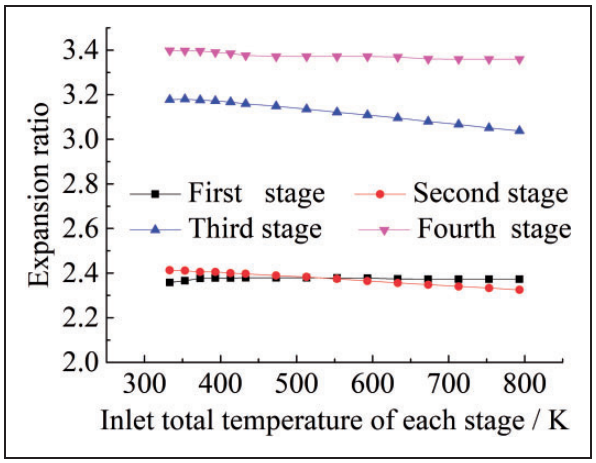

Figure 19. Variation of expansion ratio with reheating temperature.

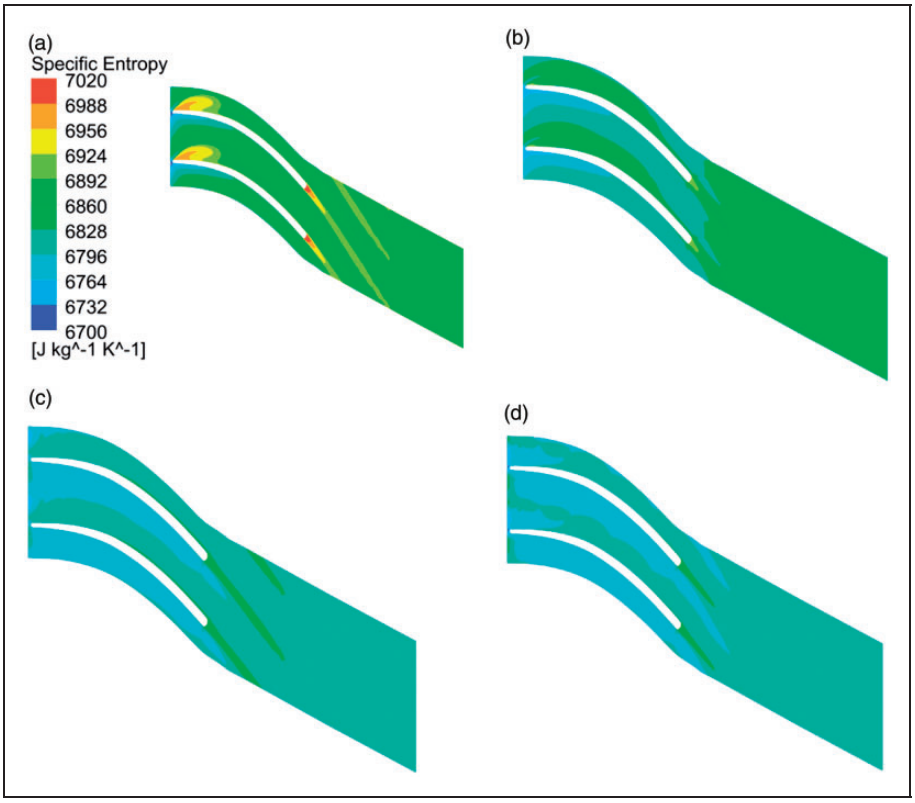

Figure 18. Rotor channel specific entropy distribution with rotational speed: (a) 60%; (b) 80%; (c) 100%; and (d) 110%.

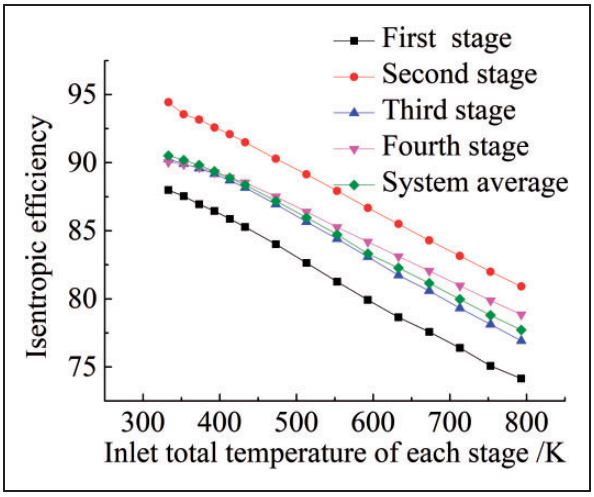

Figure 20. Variation of isentropic efficiency with reheating temperature.

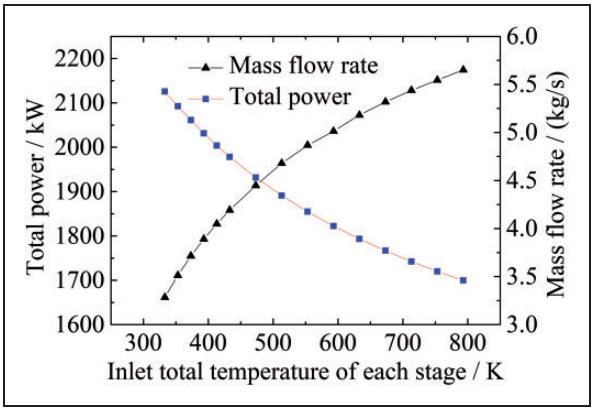

Figure 21. Variation of total power and mass flow rate with reheating temperature.

heat, geothermal energy, and so on. These heat sources temperatures are different and they can provide different reheating temperatures. Since these industrial waste heat sources are below 520 °C, several conditions utilizing temperatures from 60 °C to 520 °C are investigated.

Figure 19 shows the relationship between the expansion ratios of each stage and the reheating temperatures. It can be seen that the expansion ratios of each stage decrease slightly except that of the first stage, which is due to the increasing inter-stage pressure loss. The flow speed during the reheaters increases with the increasing reheating temperature, which leads to the increase of frictional loss and inter-stage pressure drop. This causes the decrease of expansion ratios of each stage. For the first stage, its inlet total pressure is a fixed value and the inter-stage pressure loss between first and second stage can be neglected compared to the pressure drop of first stage, so its expansion ratio is almost invariant.

Figure 20 shows the isentropic efficiencies of each stage and system average isentropic efficiency with different reheating temperatures. It can be seen that

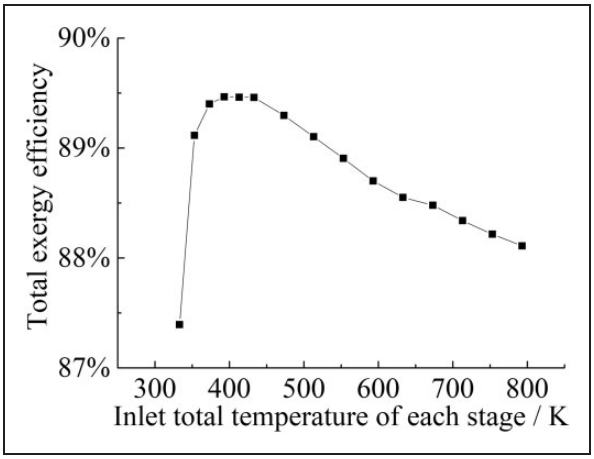

Figure 22. Variation of system total exergy efficiency with reheating temperature.

the isentropic efficiencies decrease with the increasing reheating temperature, which results from the increasing absolute velocity at the guide vane channel outlet. For a fixed rotational speed, the increasing absolute velocity will lead to higher incidence loss and the decrease of isentropic efficiencies. As each stage has the same trend, system average isentropic efficiency also reduces by the increasing the reheating temperature.

Figure 21 displays the mass flow rate and total power across different reheating temperatures. This shows clearly that the change trend of the mass flow rate is opposite to that the total power. Total power increases with the increasing reheating temperature, due to the increasing the enthalpy drop of each stage. When the inlet temperature is increased, the outlet velocity of guide vane channel will increase at the same time. Even though the incidence loss will increase, higher outlet velocity will lead to higher outlet power. However, mass flow rate decreases with the increasing reheating temperature. This is due to mass flow rate having an approximately inverse ratio relationship with the square of the total temperature of the first stage inlet when the flow in the guide vane channel reaches a critical condition.

System isentropic efficiency decreases with the increasing inlet total temperature, whereas system total power increases with the increasing inlet total temperature. An appropriate reheating temperature needs to be selected for a better overall performance. Only considering the expanding system, system total exergy efficiency is defined as

$$\eta_{ex} = \frac{W_{tot}}{Exe_{1in} - Exe_{4out} + \sum_{n=2}^{4} Exe_{(n-1)-n}} \tag{2}$$

where W_{tot} is the total power, Exe_{1in} is the inlet exergy of the first stage, Exe_{4out} is the outlet exergy of the fourth stage, and $Exe_{(n-1)-n}$ is the inter-stage exergy increase.

From Figure 22, it can be seen that the exergy efficiency reaches a maximal value when the reheating temperature is about 400 K, which means that the rated reheating temperature is appropriate. When the reheating temperature is higher than 400 K, incidence loss will increase and the exergy efficiency will decrease. When the reheating temperature is lower than 400 K, outlet temperature is less than the environment temperature. As the temperature is reheated from less than environment temperature to greater than environment temperature, even though the enthalpy increases during the reheating, it is following the exergy loss in this process. In addition to the expansion system, other factors for the selection of reheating temperature include the condition of reheating source, change of load, efficiency requirement, and so on. Further study on the selections of reheating temperature will be conducted in the future.

The performance changes of all four stages have the same trend, so only one of them needs to be analyzed to obtain their internal flow characteristics. The fourth stage is chosen and the pressure, blade load, and specific entropy distribution of the guide vane channel and rotor channel are analyzed. When the reheating temperature is increased, outlet flow angle changes minimally and its value is about 80.2°. This is mainly due to the unchanged guide vane angle. When the reheating temperature is increased, the outlet flow velocity increases almost linearly, as shown in Figure 23. This may lead to its disagreement with rotor's inlet circumferential velocity and the drop of efficiency. Increasing velocity leads to the increase of the total pressure loss, as shown in Figure 23.

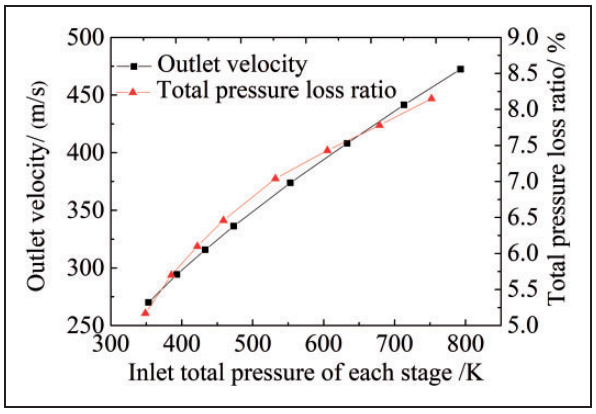

Figure 23. Guide vane channel outlet condition with reheating temperature.

Figure 24 shows the guide vane channel specific entropy distribution of 50% blade height. It is clear that the distribution is uniform in the most part. The guide vane channel loss is mainly due to the increasing friction loss between channel wall and fluid. In addition, there is a flow separation area in the exit part, which leads to the flow deterioration and the increase of total pressure loss.

The blade loads at different blade heights are shown in Figure 25. It is clear that the loads at 5% and 50% blade height increase with the increasing reheating temperature. However, the uniformity of loads is becoming poor. When the reheating temperature is increased, disagreement between the guide vane channel outlet flow's circumferential velocity and the rotor's inlet circumferential speed will increase. Fluid velocity has a sharp rise when it rounds the leading edge and enters the suction surface side. The fluid has an impulse to the pressure side due to the disagreement above and the fluid pressure increases for its velocity drop. Pressure difference between suction side and pressure side increases for the above reason. In Figure 25(c) it can be seen that the suction surface pressure at the rotor channel changes little.

The 3D fluid stream at 520 °C is shown in Figure 26. This shows that there is a vortex at the rotor channel. This vortex is generated near the suction side at the inlet part and moves towards the pressure side until it disappears. This vortex is larger when the reheating temperature is higher.

Effect of guide vane opening

When the power of SCAES needs to be changed, an efficient way is to adjust the first stage guide vane opening. The expansion ratio, mass flow rate, and

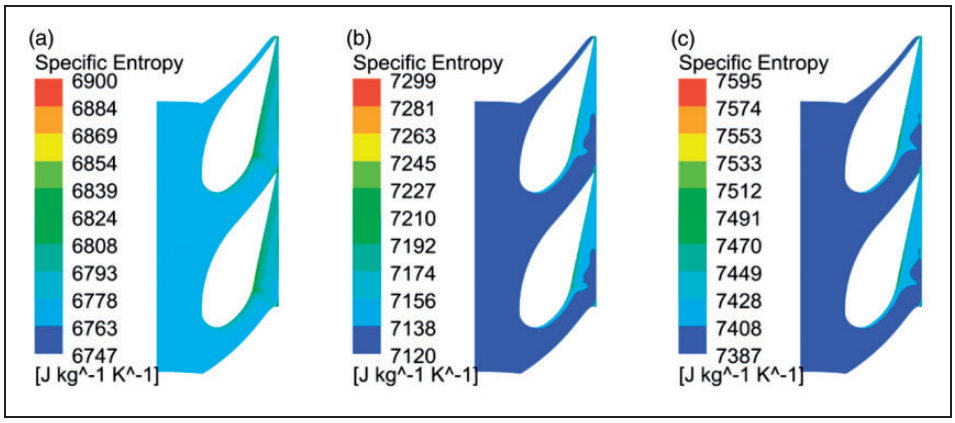

Figure 24. Guide vane channel specific entropy distribution with reheating temperature. (a) 120 °C; (b) 280 °C; and (c) 440 °C.

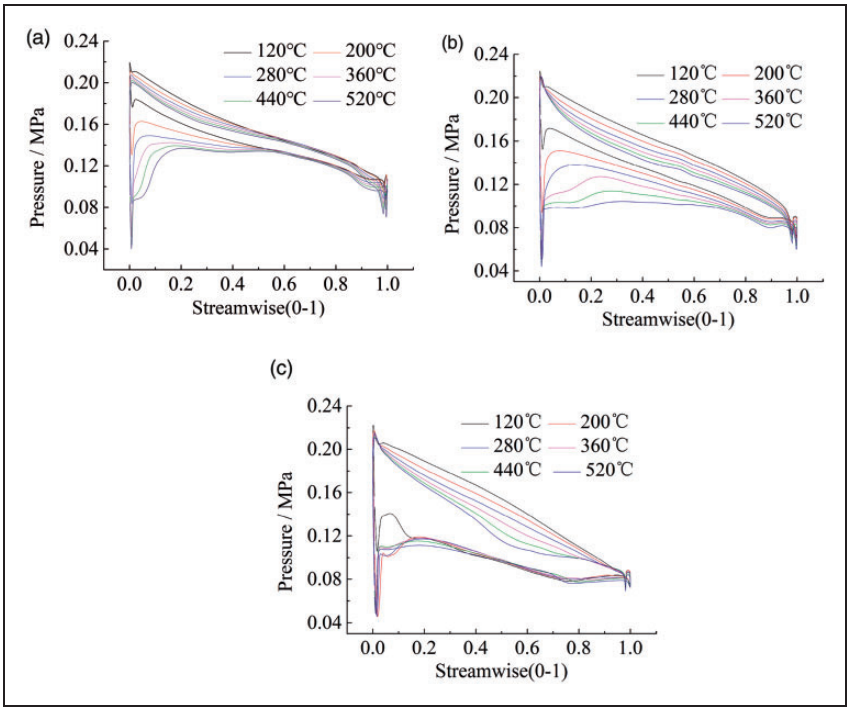

Figure 25. Blade loads at different blade heights with reheating temperature: (a) 5% blade height; (b) 50% blade height; and (c) 95% blade height.

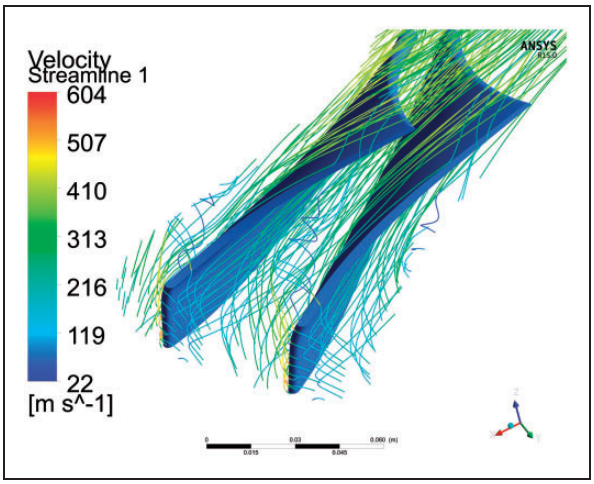

Figure 26. Rotor channel 3D fluid stream at 520°C.

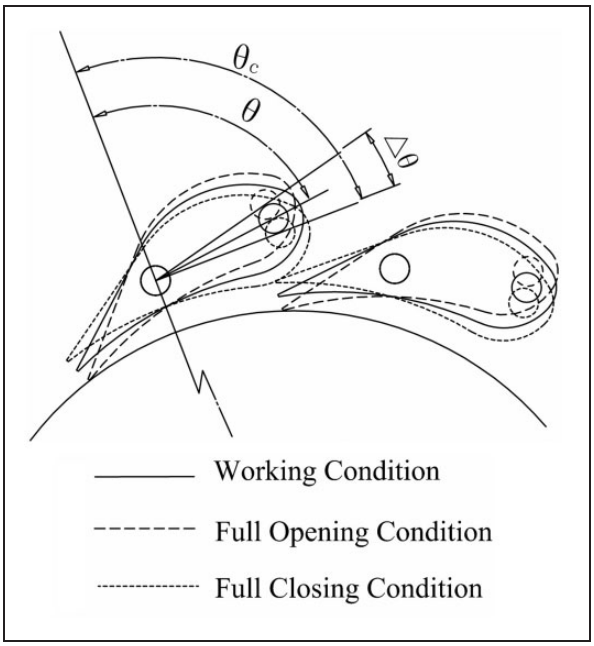

Figure 27. Schematic diagram of the guide vane opening.

efficiency of each stage will be changed in this condition. To research the influence of guide vane opening, several conditions from 30% to 80% are investigated.

The guide vane opening is defined as

$$\varepsilon = \frac{\theta_c - \theta}{\Delta\theta} \tag{3}$$

where $\Delta\theta$ is the difference between blade angle at full open condition and full close condition, θ is the blade angle at working condition, and θ_c is the blade angle at full close condition, as shown in Figure 27.

From Figure 28, it is clear that the expansion ratios of the first and fourth stage change the most, while the third stage increase only when the guide vane opening is less than 60% and the second stage is almost constant. When the guide vane opening is reduced, the smaller flow area leads to less mass flow rate. As to the fourth stage, its inlet total pressure needs to be reduced to meet the requirement of mass flow rate drop. As the outlet total pressure of the fourth stage is invariant, the expansion ratio of the fourth stage shows an opposite trend to the guide vane

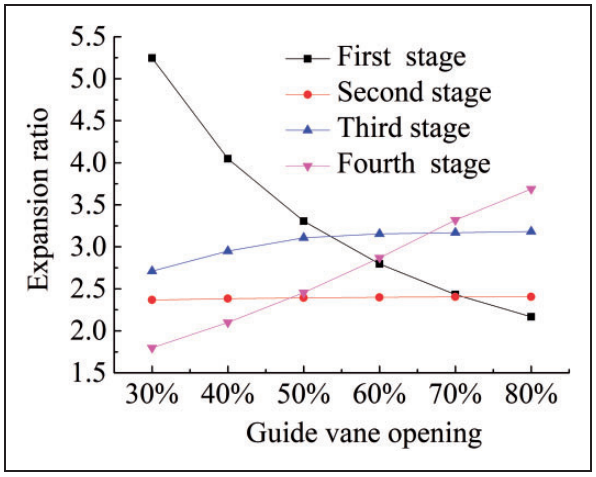

Figure 28. Variation of expansion ratio with guide vane opening.

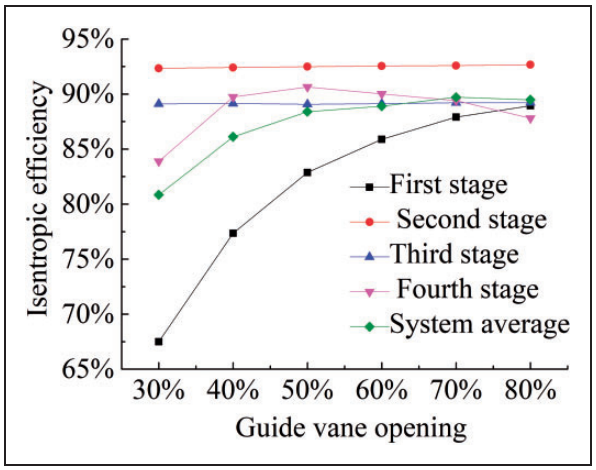

Figure 29. Variation of isentropic efficiency with guide vane opening.

opening. When the guide vane opening is above 60%, flows in the guide vane channels of second, third, and fourth stages reach a critical condition and the expansion ratios of second and third stage change little. When the guide vane opening is below 60%, flow in the guide vane channel of the third stage does not reach a critical condition. The expansion ratio of third stage reduces with the guide vane opening. When the guide vane opening is reduced, the inlet total pressure of the second stage reduces at the same time. For these reasons, the expansion ratio of the first stage has an opposite trend compared to the guide vane opening.

Similar to the obvious change of the expansion ratio, isentropic efficiencies of the first and fourth stage change the most, as shown in Figure 29. For the first stage, when the guide vane opening is increased, flow loss in the stator will diminish. In addition, outlet flow angle tends to the optimal value, so its isentropic efficiency increases quite evidently with increasing guide vane opening. For the fourth stage,

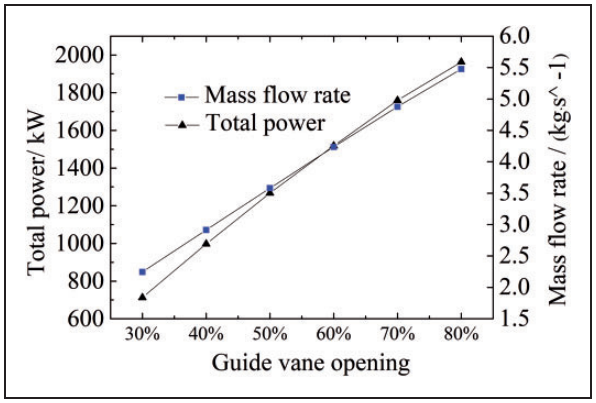

Figure 30. Variation of total power and mass flow rate with guide vane opening.

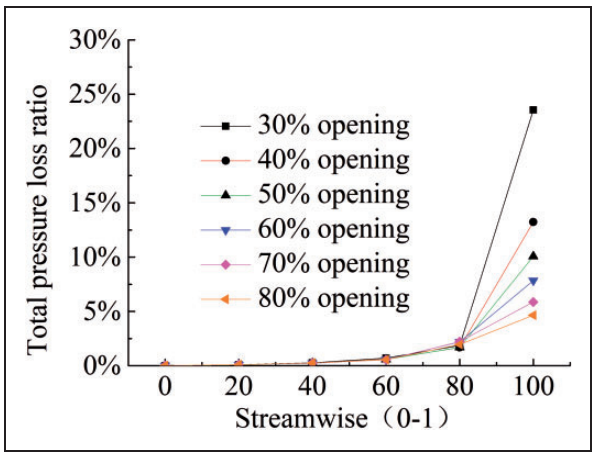

Figure 31. Total pressure loss ratio of different streamwise.

when the guide vane opening is increased, its expansion ratio is first less than the optimal value and then beyond this value, and so its isentropic efficiency increases first and then decreases with the increasing guide vane opening. For the second and third stages, their expansion ratio changes are less compared to the other stage and the expansion ratio values are near the optimal values, so their isentropic efficiencies change little. The system average efficiency increases with the guide vane opening.

From Figure 30, it can be seen that the mass flow rate and total power increase almost linearly with increasing guide vane opening. When the guide vane opening is increased, flow in the guide vane throat of the first stage reaches a critical condition. Mass flow rate is almost in direct proportion to the guide vane throat cross-sectional area in this condition. As the guide vane throat cross-sectional area is almost in direct proportion to the guide vane opening, mass flow rate is also almost in direct proportion to the guide vane opening. Even though the isentropic efficiency of the first and fourth stages change a lot with the guide vane opening, the change of system average isentropic efficiency is slight and it is nearly in proportion to the guide vane opening.

The change of the first and fourth stages is more obvious compared to the other stages when the guide vane opening is reduced from 80% to 30%. Variation of the fourth stage is mainly due to the reduced inlet total pressure and this condition has been investigated above. Change in the first stage is mainly due to the reduced guide vane opening, so the internal flow of the first stage will be researched next.

The reduced guide vane opening leads to the increase of the outlet flow angle and velocity of the guide vane channel. Guide vane channel pressure loss mainly occurs at the last 20% of the channel, as shown in Figure 31.

When the guide vane opening is smaller, the increasing disagreement between the outlet flow's circumferential velocity and rotor's circumferential linear velocity would increase the flow loss of the guide vane channel, as shown in Figure 32. This phenomenon is especially significant at small guide vane opening. When the opening is smaller, the flow mass leaking from the blade tip and root clearance to the main channel is greater. The mixing of the leaking flow and the main flow leads to increasing flow loss and inconsistent outlet flow.

Efficiency drops rapidly with reduced guide vane opening. To investigate the reason for this

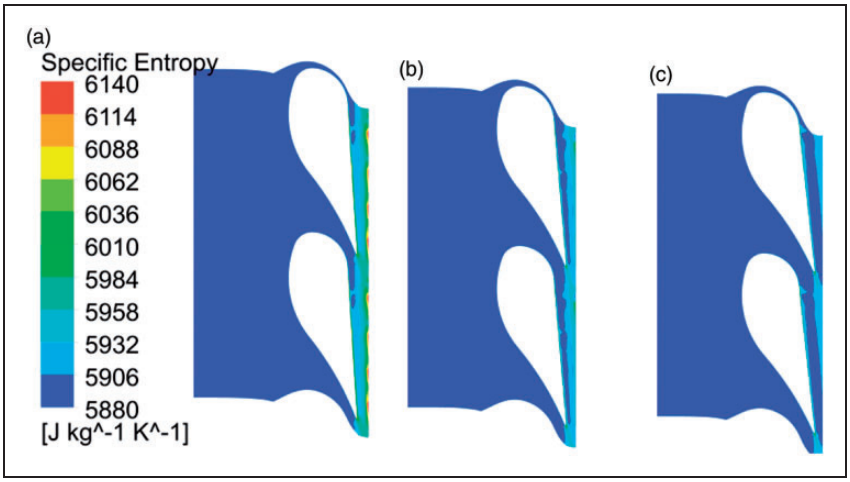

Figure 32. Contour of specific entropy at 50% span with different guide vane openings: (a) 30% opening; (b) 40% opening; and (c) 50% opening.

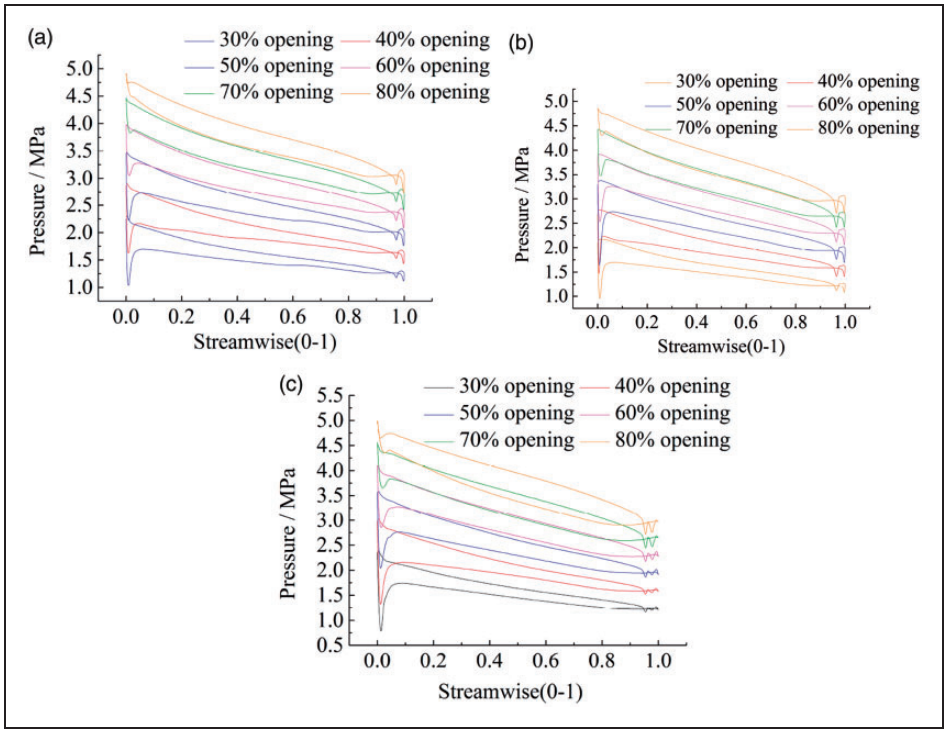

Figure 33. Blade load with different blade heights at different openings: (a) 5% blade height; (b) 50% blade height; and (c) 95% blade height.

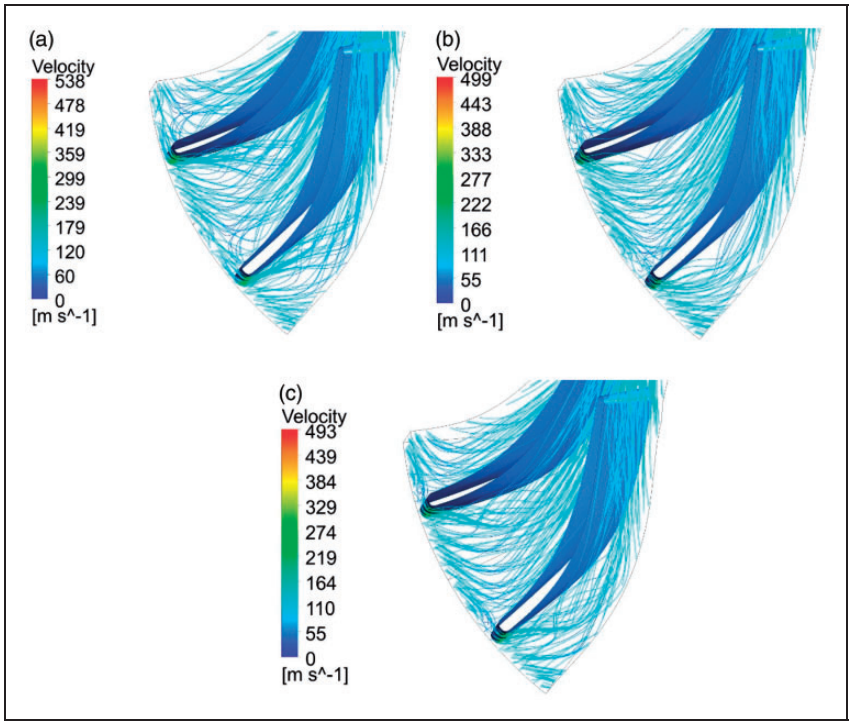

Figure 34. Rotor channel 3D fluid stream: (a) 30% opening; (b) 40% opening; and (c) 50% opening.

phenomenon, blade loads with different blade heights at different guide vane openings are obtained, as shown in Figure 33. It is clear that the pressure, pressure difference, and pressure difference uniformity at streamwise increase with the increase in the opening.

When the guide vane opening is reduced, a vortex is generated near the suction side at the inlet part of the rotor channel, as shown in Figure 34. The vortex leads to the drop of fluid velocity and the increase of static pressure in this region, which leads to the drop of pressure difference and power. When the guide vane opening is reduced, some main stream even flows from the pressure side to the suction surface, which leads to the increase in the suction side pressure and decrease in the pressure difference and power. The loss increase and power reduce lead to the drop of efficiency due to the above reasons.

Conclusion

In this paper, concerning the SCAES system, the overall performance and internal flow characteristics of variable operating conditions of the multistage reheating radial inflow turbine are analyzed with integral numerical calculation. The following conclusions can be drawn from the analyses:

1. For the multistage reheating radial inflow turbines, influences of rotational speed and reheating temperature on the expansion ratio can be considered to be negligible. When the inlet total pressure of the first stage is reduced, changes in the expansion ratios from the first stage to the fourth stage increase gradually when compared to the rated condition. When the guide vane opening is increased, expansion ratio of the first stage and fourth stage change the most and the change in trend of the first stage is different from the other stages.
2. Isentropic efficiencies of each stage and system increase with the increase in the rotational speed. However, they are reduced when the reheating temperature is increased. When the inlet total pressure of the first stage is reduced, isentropic efficiencies of each stage change little except for the fourth stage. System isentropic efficiency decreases about 1% when the inlet total pressure is reduced from 7 MPa to 3 MPa and the fourth stage isentropic efficiency decreases about 7%. When the guide vane opening is increased, the isentropic efficiency of the first stage increases all the time but the fourth stage first increases and then decreases. System isentropic efficiency decreases about 4% when guide vane opening is reduced from 80% to 30%.
3. Total power is almost in proportion to the inlet total pressure of the first stage, guide vane opening and it reduces with the decline of rotational speed. When the reheating temperature is increased from 60 °C to 520 °C, the system total power increases by about 105%.

Declaration of Conflicting Interests

The author(s) declared no potential conflicts of interest with respect to the research, authorship, and/or publication of this article.

Funding

The author(s) disclosed receipt of the following financial support for the research, authorship, and/or publication of this article: This work was supported by the National Key R&D Plan (2017YFB0903602), National Natural Science Foundation of China (51522605), Transformational Technologies for Clean Energy and Demonstration, Strategic Priority Research Program of the Chinese Academy of Sciences (XDA21070200), The Frontier Science Research Project of CAS (QYZDB-SSW-JSC023), and Beijing Science and Technology Plan (D161100004616001, D161100004616002).

References

1. Liu X, Lin C and Rao Z. Diffusion and thermal conductivity of the mixture of paraffin and polystyrene for thermal energy storage: A molecular dynamics study. *J Energy Inst* 2017; 90: 534–543.
2. Du YP and Ding YL. Cold-to-electricity conversion using a piston based engine in cold energy storage (CES) system, part one: A theoretical study. *J Energy Inst* 2017; 90: 661–671.
3. Chen HS, Cong TN, Yang W, et al. Progress in electrical energy storage system: A critical review. *Prog Nat Sci* 2009; 19: 291–312.
4. Swider DJ. Compressed air energy storage in an electricity system with significant wind power generation. *IEEE Trans Energy Convers* 2007; 22: 95–102.
5. Guo H, Xu YJ, Chen HS, et al. Thermodynamic analytical solution and exergy analysis for supercritical compressed air energy storage system. *Appl Energy* 2017; 199: 96–106.
6. Zhang XH, Chen HS, Liu JC, et al. Research progress in compressed air energy storage system: A review. *Energy Storage Sci Technol* 2012; 1: 26–40.
7. Rodgers C. The characteristics of radial turbines for small gas turbines. In: *ASME turbo expo 2003, collocated with the 2003 international joint power generation*, Atlanta, Georgia, USA, 2003, pp.657–667.
8. Hung TC, Shai TY and Wang SK. A review of organic rankine cycles (ORCs) for the recovery of low-grade iste heat. *Energy* 1997; 22: 661–667.
9. Bruno JC, Ortega LV and Coronas A. Integration of absorption cooling systems into micro gas turbine trigeneration systems using biogas: Case study of a sewage treatment plant. *Appl Energy* 2009; 86: 837–847.
10. Dambach R, Hodson HP and Huntsman I. 1998 Turbomachinery Committee Best Paper Award: An experimental study of tip clearance flow in a radial inflow turbine. *J Turbomach* 1999; 121: 644–650.
11. Hiet GF and Johnston IH. Experiments concerning the aerodynamic performance of inward flow radial turbines. *Proc Instn Mech Engrs* 1964; 178.
12. Kofskey MG and Haas JE. Effect of reducing rotor blade inlet diameter on the performance of a 11.66-Centimeter radial-inflow turbine. NASA Report, Lewis Research Center, 1973.
13. Watanabe I, Ariga I and Mashimo T. Effect of dimensional parameters of impellers on performance characteristics of a radial-inflow turbine. *J Eng Gas Turbines Power* 1971; 93: 81–102.
14. Simonyi PS, Roelke RJ, Stabe RG, et al. Aerodynamic evaluation of two compact radial-inflow turbine rotors. NASA STI/Recon Technical Report 3514, 1995.
15. Li Y and Zheng Q. Numerical simulation of a multistage radial inflow turbine. *Proceedings of ASME turbo expo 2006: Power for land, sea, and air*. Barcelona, Spain, 2006, pp.1141–1148.
16. Li Y, Zheng Q and Sun L. The effect of partial admission on multistage radial inflow industrial steam turbine. *ASME turbo expo 2009: Power for land, sea, and air*. 2009, pp.623–629.
17. Hamdi F, Seo J and Han S. Numerical investigation of an organic Rankine cycle radial inflow two-stage turbine. *J Mech Sci Technol* 2017; 31: 1721–1728.
18. Zhang XH, Chen HS, Yan XH, et al. Analysis of an air poared engine system using a multi-stage radial turbine. *Entropy* 2013; 15: 1186–1201.
19. Zhang XH. *Multistage radial turbine for supercritical compressed air energy storage system*. Dissertation, University of Chinese Academy of Sciences, Beijing, 2014.
20. Huang LY, Wen JX, Karayiannis TG, et al. CFD modelling of fluid flow and heat transfer in a shell and tube heat exchanger. *Phoenics J Comput Fluid Dyn Appl* 1996; 9: 181–209.

Appendix

Notation

Exe	exergy
W	power
ΔH	enthalpy drop
ε	guide vane opening
η_{ex}	system total exergy efficiency
$\eta_{tot-isp}$	system average isentropic efficiency
θ	blade angle